Base Algorithms of Environment Maps and Efficient Occupancy Grid Mapping on Embedded GPUs

Jörg Fickenscher[1], Frank Hannig[1], Jürgen Teich[1] and Mohamed Essayed Bouzouraa[2]
[1]*Department of Computer Science, Friedrich-Alexander University Erlangen-Nürnberg (FAU), Germany*
[2]*Concept Development Automated Driving, AUDI AG, Ingolstadt, Germany*

Keywords: Autonomous Driving, Environment Maps, GPGPU.

Abstract: An accurate model of the environment is essential for future Advanced Driver Assistance Systems (ADASs). To generate such a model, an enormous amount of data has to be fused and processed. Todays Electronic Control Units (ECUs) struggle to provide enough computing power for those future tasks. To overcome these shortcomings, new architectures, like embedded Graphics Processing Units (GPUs), have to be introduced. For future ADASs, also sensors with a higher accuracy have to be used. In this paper, we analyze common base algorithms of environment maps based on the example of the occupancy grid map. We show from which sensor resolution it is rational to use an (embedded) GPU and which speedup can be achieved compared to a Central Processing Unit (CPU) implementation. A second contribution is a novel method to parallelize an occupancy grid map on a GPU, which is computed from the sensor values of a lidar scanner with several layers. We evaluate our introduced algorithm with real driving data collected on the autobahn.

1 INTRODUCTION AND RELATED WORK

Motivation: Since the last years, there is an enormous hype about autonomous driving and ADASs. To make it happen, e.g., driving autonomously on a highway, a vehicle needs an accurate model of its environment. These models have to contain all static and dynamic objects in the vehicle surroundings, as well as the own vehicle position. To create such a model, sensors with a high resolution are necessary. These sensors deliver enormous amounts of data, which have to be fused and processed to create an accurate environment map. Nowadays, the processors in ECUs, which are mostly single-core CPUs, struggle to provide enough computing power for these tasks. Here, new emerging architectures appear. One of the most promising is the use of GPUs in automotive ECUs. Today's hardware performance gains are mostly achieved through more cores and not through a higher single-core performance. Here, GPUs perfectly fit in, with their hundreds of cores in embedded systems compared with mostly quad-core CPUs in embedded systems. To use such architectures, it is necessary to switch from the predominant single-threaded programming model to a multi-threaded programming model. Thus, the software has to be adjusted, parallelized were possible or entirely new written for these platforms. Another key point is that not only new hardware platforms but also new sensors with a higher accuracy are necessary for future ADASs. One important research question is, we look into in this paper, how the algorithms scale for larger sensors, and what is the sweet spot of the architecture (CPU/GPU) and mapping. Often, if an environment map is created, there are several base algorithms, which are necessary, no matter which type of environment map is created. As a first contribution, we analyze in this paper, how the base algorithms scale with different sensor resolutions on different hardware platforms, which is very important knowledge for Original Equipment Manufacturers (OEMs). In former times, sensors scanned only one vertical layer of the environment. However, they have not only an increased resolution in the horizontal but recently also in the vertical direction. Since the measurements in the vertical direction may be dependent, it is not easy to evaluate such sensor measurements in parallel on a GPU. We purpose a novel parallel evaluation of lidar scanner data on the example of the very well-known environment map, the occupancy grid map. To show the capability of our approach, we evaluate it with collected real-time data by an experimental car.

In the next paragraph, we discuss related work. In Section 2, we give an overview of the base algorithms of environment maps and introduce our new method for the parallelization of an occupancy grid map on a GPU. Subsequently, we evaluate our approach in Section 3. Finally, we conclude our paper in Section 4.

Related Work: Creating environment maps, like the

Fickenscher, J., Hannig, F., Teich, J. and Bouzouraa, M.
Base Algorithms of Environment Maps and Efficient Occupancy Grid Mapping on Embedded GPUs.
DOI: 10.5220/0006677302980306
In *Proceedings of the 4th International Conference on Vehicle Technology and Intelligent Transport Systems (VEHITS 2018)*, pages 298-306
ISBN: 978-989-758-293-6

occupancy grid map, introduced by Elfes (Elfes, 1989) and Moravec (Moravec, 1988), is a common problem in robotics. They used their approach to describe the environment, which was static, for a mobile robot. Also, grid maps are used in robotics for Simultaneous Localization and Mapping (SLAM) problems like in (Grisettiyz et al., 2005) or multiple object tracking (Chen et al., 2006). Most of the approaches use only a 2D occupancy grid, but some works extended it to a third dimension (Moravec, 1996). The problem with 3D methods is the high memory consumption, which was addressed by (Dryanovski et al., 2010). Since the basic idea of robotics and autonomous vehicles is very similar, it is not surprising that the concept of occupancy grid maps was also introduced to the automotive sector. The difference to the automotive context is, that for robotics often a static map is created only once, whereas for vehicles the map has to be continuously updated due to the dynamic environment. In (Badino et al., 2007), the authors introduced an occupancy grid for the automotive domain to compute the free space of the environment. Occupancy grid maps are also used for lane detection (Kammel and Pitzer, 2008) or path planning (Sebastian Thrun, 2005). Often laser range finders are used to create occupancy grid maps (Homm et al., 2010) (Fickenscher et al., 2016), as we consider in this paper, but it is also possible to use radar sensors (Werber et al., 2015) to create such maps. Since creating occupancy grid maps can be very compute-intensive, it was parallelized on a GPU (Homm et al., 2010). They used in their approach a desktop PC, as proof of concept. However, space and energy requirements are far away from a realistic ECU. In this paper, we use an embedded platform, which is much more similar to a later ECU design. Yguel et al. (Yguel et al., 2006) used several laser range finders, but only with one vertical layer and they did their experiments also on a desktop computer. In (Fickenscher et al., 2016), the occupancy grid map was parallelized on an embedded GPU. In this approach, a laser sensor with only one layer in the vertical was used. In this paper instead, a sensor with several vertical layers is used. Hereby the accuracy of the occupancy grid map is enormously increased but also the computational effort rises proportionally.

2 FUNDAMENTALS

In this section, a brief overview of creating environment maps, especially an occupancy grid map is given. Then, our very efficient algorithm to create an occupancy grid is described and its parallelization. Also, the specific properties of embedded GPUs are shortly summarized. Further, differences in parallelizing the algorithm on a GPU, instead on a CPU are described.

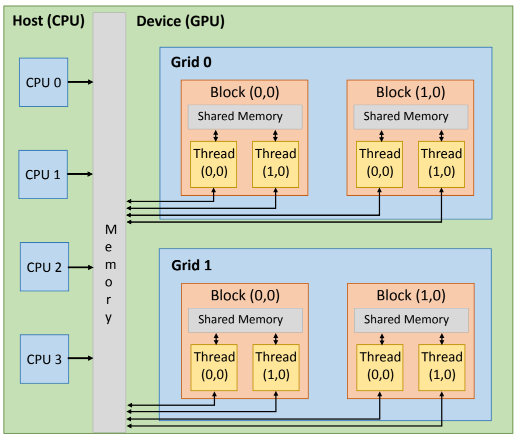

Figure 1: Structural overview of the CUDA programming model for an embedded GPU.

2.1 Programming an Embedded GPU

The main purpose of GPUs has been rendering of computer graphics, but with their steadily increasing programming and memory facilities, GPUs recently become attractive for also accelerating compute-intensive algorithms from other domains. GPUs show their strengths, if the algorithm has a high arithmetic density and could be parallelized in a data-parallel way. However, the hardware architecture of a GPU and a CPU is quite different. A GPU embodies at hardware level several *streaming processors*, which further contain processing units. Such a streaming processor manages, spawns, and executes the threads. Those threads are managed in groups of 32 threads, so-called *warps*. In a warp, every thread has to execute the same instruction at the same time. E.g., if there is a branch, for which only half of the threads, the statement is evaluated *true*, the other half of the threads has to wait. As illustrated in Figure 1, threads are combined to logical blocks, and these blocks are combined to a logical grid. In 2006 (NVIDIA Corp., 2016b), Nvidia introduced the framework CUDA to ease the use of GPUs for general purpose programming. Program blocks, which should be executed in parallel, are called *kernels*. Those kernels can be executed over a range (1D/2D/3D) specified by the programmer. For a range, which has n elements, n threads are spawned by the CUDA runtime system. The programming model for the parallelization of an algorithm is also different. On a CPU, parallel threads are executed on different data, and every thread processes different instructions. On a GPU instead, every thread executes the same instruction at the same time on different data. This model is called Single Instruction Multiple Threads (SIMT). The main difference bet-

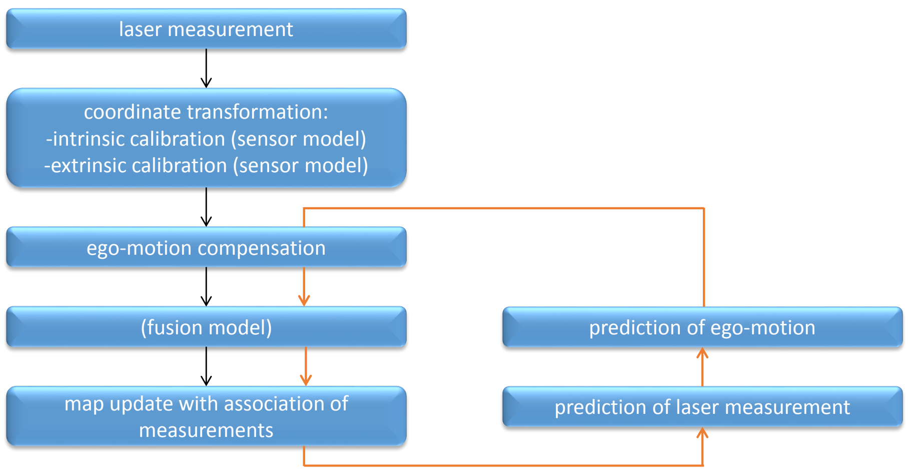
laser measurement
coordinate transformation:
-intrinsic calibration (sensor model)
-extrinsic calibration (sensor model)
ego-motion compensation
(fusion model)
map update with association of measurements
prediction of ego-motion
prediction of laser measurement

Figure 2: Overview of the sub-algorithms which are necessary to create an environment map.

ween a discrete desktop GPU and an embedded GPU is the memory system. On an embedded GPU, like illustrated in Fig. 1, there is no separation between the main memory of the system and the GPU memory, like on a desktop computer. So on an embedded, GPU no data has to be explicitly copied from the main memory to the GPU memory to execute an algorithm on that data on the GPU.

2.2 Base Algorithms of ADAS

Environment maps represent the surrounding of a car and are always necessary for automated driving systems. No matter which environment map is used, there are a few base algorithms, which are always necessary, e.g., the compensation of the ego-motion, coordinate transformations and updating the environment map. In Figure 2 an overview of the different base algorithms, which are necessary to create an environment map, are given. The brown arrows indicate the predict and update step of the Kalman filter (Kalman, 1960), which is independent of the other base algorithms. In the following, these algorithms are further described.

2.2.1 Coordinate Transformation

To create an environment map out of the sensor measurements, the characteristics of the *sensor model* have to be considered. A sensor model consists of *intrinsic* and the *extrinsic* parameters. For example, if a fisheye camera is used, the intrinsic calibration process is to transform the stream with a strong visual distortion into a stream with straight lines of perspective. Since the sensors have different positions on the vehicle, all the measurements of the sensors have to be transformed into one coordinate system. This is the extrinsic calibration process. First, they have to be transformed into Cartesian coordinates because that is the coordinate system of the environment map. The sensor measurements of, e.g., laser scanners are normally in polar coordinates r and φ. Therefore, the measurements have to be transformed from polar to Cartesian coordinates with $x = r\cos\varphi$ and $y = r\sin\varphi$. The fisheye camera has a spherical coordinate system and with $x = r\sin\Theta\cos\varphi$, $y = r\sin\Theta\sin\varphi$ and $z = r\cos\Theta$ it can be transformed to Cartesian coordinates. The origin of the coordinate system for environment maps is often set to the middle of the rear axle of the vehicle. So all the coordinate systems with different origins have to be transformed to a coordinate system with one origin. We use homogeneous coordinates to do this transformation.

2.2.2 Ego-motion Compensation

By creating an environment map, it is also necessary to compensate the ego-motion of the own vehicle. In principle, there are two approaches to do that. One is to compensate the sensor measurements by the ego-motion directly. For that, usually homogeneous coordinates are used, because the translation and rotation can be done with one matrix. The matrix is used for every laser beam to compensate the ego-motion.

The other method is to shift the environment map by the ego-motion of the own vehicle. E.g., if an occupancy grid map is used the ego-motion can be compensated by rotating the vehicle on the map and shifting two pointers, one for the movement in x-direction and one for the movement in y-direction, like explicitly described in (Fickenscher et al., 2016).

2.2.3 Fusion Model

To get a detailed knowledge about the vehicle environment, different sensors are necessary. The measurements of different sensors have to be put together, to have an entire picture of the environment in one map. In the *fusion model*, this step is done. First, the different data has to be synchronized in time, because different sensors have a different update interval. In a second step, the data has to be merged together. That is the speed of a vehicle, measured by a radar sensor, is combined with the detected vehicle by a laser scanner.

2.2.4 Kalman Filter

Sensor measurements often contain some noise or other inaccuracies, e.g., statistical outliers. The Kalman filter (Kalman, 1960) is used to estimate values, e.g., the speed of the own vehicle, based on several past measurements. Those estimations are combined with the actual measurement. As a result of this the actual measurement is smoothed, to get rid of challenges mentioned above.

2.2.5 Update Environment Map

To update an environment map, the new sensor measurements have to be entered into the old map. Therefor, it is necessary to associate the objects in the environment map with the new measurements from the sensor. It has to be decided, which measurement belongs to which object or if there is a belonging object to a measurement or not and a new one has to be created. A simple algorithm for this challenge would be for example Global Nearest Neighbor (GNN), based on the work of Cover and Hart (Cover and Hart, 2006). Here, for every already tracked object the distance to all measured objects is calculated and then, the measurement is associated with the closest distance to a tracked object. A more sophisticated approach is the probabilistic data association filter (PDAF) (Bar-Shalom et al., 2009) (Musicki and Evans, 2004). Commonly, a probabilistic data association (PDA) algorithm computes the association probabilities, taking into account the uncertainties of the measurement, to the targets being tracked for each measurement. Finally, the two values, usually probabilities if there is an obstacle or not, have to be merged together. For an occupancy grid map the process is described in Section 2.3, but for other types of environment maps it is similar.

2.3 Occupancy Grid Mapping

Occupancy grid mapping is very famous in robotics, due to its easy principles. The environment is rasterized in equally sized squares, so-called cells, and for every cell, a probability is calculated, how likely the cell is occupied. The golden standard (Sebastian Thrun, 2005) is to calculate the posterior p of the single cells m_i of the map m from $z_{1:t}$ and $x_{1:t}$:

$$p(m_i|z_{1:t}, x_{1:t}) \in [-1,1]_{\mathbb{R}} \tag{1}$$

Hereby, $z_{1:t}$ are the sensor measurements and $x_{1:t}$ the positions of the vehicle, from time 1 to time t. To avoid numerical pitfalls close to zero or one, the so-called log-odds form is used:

$$p(m_i|z_{1:t}, x_{1:t}) = \log \frac{p(m_i|z_{1:t}, x_{1:t})}{1 - p(m_i|z_{1:t}, x_{1:t})} \tag{2}$$

Applying to Equation (2) the Bayes' rule, in order to eliminate some hard to compute terms, leads to:

$$p(m_i|z_{1:t}, x_{1:t}) = \frac{p(z_t|z_{1:t}, m_i) \cdot p(m_i|z_{1:t})}{p(z_t|z_{1:t})} \tag{3}$$

If a cell is occupied, it is noted as $p(m_i) = 1.0$ and if a cell is empty, it is noted as $p(m_i) = 0.0$.

2.4 Efficient Occupancy Grid Mapping Algorithm

For a precise occupancy grid map, it is necessary to have a laser scanner with several layers. The reason for this is that on the one hand a laser scanner with only one layer cannot detect objects with small heights. On the other hand, also the accuracy increases for objects, that are high enough to be detected by a laser beam with one layer, because not every laser channel is reflected accurately. So, if an object is hit by several laser beams in one vertical layer, it is more likely, that one laser beam is reflected properly. In Algorithm 1, the coordinate transformation from polar to Cartesian coordinate space is done, including the sorting of the sensor measurements. Here, the three vertical sensor measurements are sorted by their length with a bubble sort algorithm. Therefore, over all laser channels N_c is iterated. The reason is, that then, in the update Algorithm 2, not all measurements have to be evalu-

Algorithm 1: Coordinate transformation with sorting the measurements according to the distance of the sensed objects.

```
 1: function SORTANDTRANFORMATION
    (LaserMeasurment, SortedTransformedMeasurement)
 2:     for all $i \in [0, N_c - 1]$ do
 3:         bubbleSort $(m_{i,0}, \ldots, m_{i,N_l-1})$
 4:     end for
 5:     for all $i \in [0, N_c - 1]$ do
 6:         for all $j \in [0, N_l - 1]$ do
 7:             if $m_{i,j} < threshold$ then
 8:                 Coordinate transformation from polar to
                    Cartesian $M_{i,j}$
 9:             end if
10:         end for
11:     end for
12: end function
```

ated. In a second step, the measurement is transformed from polar to Cartesian coordinate space, by iterating over all laser layers N_l and laser channels N_c.

The actual update of the occupancy grid map is shown in Algorithm 2. At first, it is checked, if the measurement is valid or not. A measurement can be invalid, e.g., if it is very close to the sensor origin, because there is some dirt on the sensor. With the second *if-statement*, it is checked, if all three vertical measurements of one horizontal layer are free. This means, there were no obstacles, on the particular laser beam, within the maximum range of the sensor. We have to check only the first measurement, because in Algorithm 1, we sorted them by the distance to the measured object. If that is the case, only one vertical measurement is put into the map with a Bresenham algorithm (Bresenham, 1965).

In the other case, the sensor measured an object closer than the maximum range of the sensor and therefore, the occupancy grid map is updated, with all three vertical measurements of one horizontal layer, also by a Bresenham algorithm. So, the cells between a measured object and the sensor are updated three times with a probability that indicates, if they are free. Instead, if there is no object, the cells are updated only once wit a probability that they are free. The reason for that is, that if the there is an object recognized by the sensor it is very likely, that there is no other obstacle in front of this detected object. If there is no measurement at all in one channel, the likelihood is less, that there is not an object. After that, it is also distinguished between static and dynamic objects.

Algorithm 2: Update algorithm of the occupancy grid map.

```
 1: function UPDATEALGORITHM
    (SortedTransformedMeasurement, OccupancyGridMap)
 2:     for all $i \in [0, N_c - 1]$ do
 3:         if $m_{i,0}$ != valid then
 4:             break
 5:         end if
 6:         if $m_{i,0}$ channel free then
 7:             Bresenham algorithm ($m_{i,j}$)
 8:             break
 9:         end if
10:         for all $j \in [0, N_l - 1]$ do
11:             Bresenham algorithm ($m_{i,j}$)
12:             classify dynamic and static objects
13:         end for
14:     end for
15: end function
```

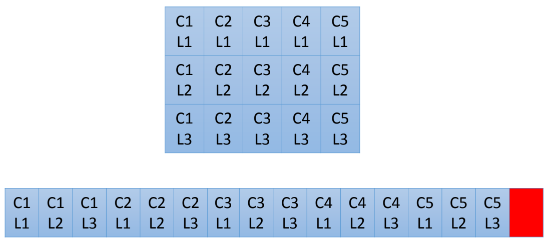

Figure 3: The upper part of the figure shows the normal arrangement of the laser scan. The lower part of the figure shows the arrangement in a GPU *warp*. *C* specifies a laser channel of a horizontal layer, and *L* specifies a laser channel of a vertical layer, e.g., *C1L1* is the first laser channel of the first vertical layer.

2.5 Parallelization Occupancy Grid Map Updated

A difficult challenge to be solved is the parallelization of an occupancy grid map update is the dependence of vertical layers (L) of one horizontal channel (C). E.g., the dependency between the laser measurements $C1L1$, $C1L2$ and $C1L3$ as shown in Figure 3. Normally, the threads in a CUDA kernel would be ordered in a 2D grid block, like shown in the upper graphics of Figure 3. One dimension would be the channels of the laser scanner and the other dimension, the layers of the laser scanner. But this is not possible because then the measurements of the layers of one channel would be in different warps. Since the order of execution of different warps cannot be determined by the CUDA programming model, the dependencies between the layers would not be respected. So the CUDA threads have to be ordered in an appropriate way, as shown in Figure 3. The CUDA threads are now ordered in an 1D grid block. Thereby, the threads, which examine the layer of one channel are ordered one after the other in one half warp. Since the layers of one channel are now in one half warp, it can be guaranteed that the dependencies are respected. The price to pay for this method is that the layers of one channel have to fit in one half warp or one full warp, depending on the architecture. This means, the maximum number of vertical layers of a lidar scanner is limited to 32 on modern architectures and on older GPUs to 16, due to a warp size of 32 or 16 for half warps. The reason for the higher number of vertical layers on modern GPU architecture is that on these architectures both half warps are executed consecutively. Also, only a multiple of the number of layers can be put into one warp. In our example, five channels with the corresponding three layers could be put in one half-warp. This means, 15 CUDA threads of the half-warp are executing the algorithm, while the 16*th* CUDA thread cannot be assigned a task. This 16*th* CUDA thread is marked red in Figure 3.

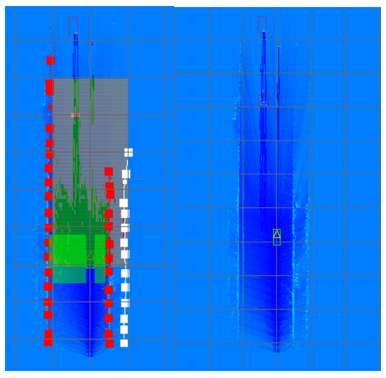

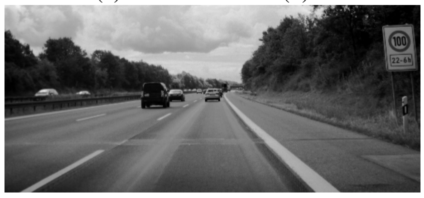

Figure 4: One of the scenarios, that was used to test our algorithm. (a) shows the grid map with annotations, like dynamic and static objects. (b) shows the grid map without notations. (c) shows the grayscale video image of the grid maps in (a) and (b).

3 EVALUATION

3.1 Experimentation Platform

We used two platforms in our experiments. A desktop PC, equipped with an Intel i7-3960X and an Nvidia 680 GTX GPU. The CPU has six cores with Hyper-Threading and a maxiumum clock frequency of $3.9GHz$. The GPU on the desktop PC has 1536 CUDA cores and $1058MHz$. As an embedded platform, an Nvidia Jetson K1 board (NVIDIA Corp., 2016a) is used. It embodies an ARM Cortex-A15 quad-core CPU with $2.3GHz$ and a Tegra Kepler GPU with 192 CUDA cores, at $850MHz$. This platform has typically only a power consumption under workload of $8-10$W. So it can be cooled passively, which is important for ECUs in vehicles. Furthermore, the same GPU is also used by the AUDI AG in their zFAS (Audi AG, 2016). We did our experiments with real data, collected on a highway by a car equipped with a laser scanner in the front of a car. One of the driving scenarios is shown in Figure 4. The laser scanner has a resolution of 581 channels in the width and 3 layers in the height. For each experiment, we averaged the measurements of 100 runs.

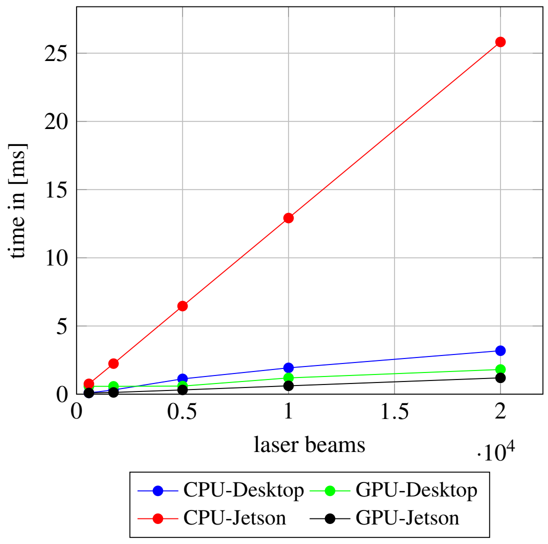

Figure 5: Each single laser beam of the measurement is transformed from polar to Cartesian space in homogeneous coordinates.

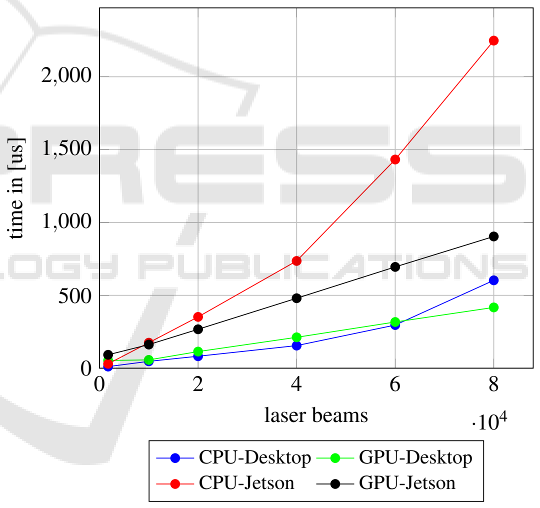

Figure 6: Each single laser beam of the measurement is compensated by the ego-motion of the own vehicle.

3.2 Experiments

3.2.1 Base Algorithms

One of the base algorithm, which is needed for creating environment maps is the coordinate transformation from polar to Cartesian coordinate space. For every laser measurement, one CUDA thread was created on the GPU. The results of that transformation, for different sensor resolutions, are illustrated in Figure 5.

For a small number of laser beams, the CPUs on both evaluation platforms are faster. The reason is that the usage of a GPU always has a slight overhead,

Table 1: Each single laser beam of the measurement is transformed from polar to Cartesian space in homogeneous coordinates on the Jetson K1 board. The results are in milliseconds [ms].

Number of laser channels	K1-CPU	K1-GPU
1743	min: 0.029	min: 0.024
	max: 0.662	max: 0.177
	avg.: 0.038	avg.: 0.093
	med.: 0.030	med.: 0.092
10000	min: 0.171	min: 0.154
	max: 6.638	max: 0.348
	avg.: 0.287	avg.: 0.168
	med.: 0.175	med.: 0.162
20000	min: 0.343	min: 0.257
	max: 8.011	max: 0.367
	avg.: 0.513	avg.: 0.271
	med.: 0.352	med.: 0.267
40000	min: 0.690	min: 0.419
	max: 8.389	max: 0.613
	avg.: 1.116	avg.: 0.512
	med.: 0.736	med.: 0.480
60000	min: 1.137	min: 0.628
	max: 11.973	max: 0.734
	avg.: 2.291	avg.: 0.693
	med.: 1.432	med.: 0.695
80000	min: 1.876	min: 0.836
	max: 12.255	max: 0.939
	avg.: 3.513	avg.: 0.904
	med.: 2.248	med.: 0.904

e.g., memory transfers or allocating of GPU memory. Between 581 and 5000 laser beams, the execution time on the desktop GPU is more or less the same. This is due to the low utilization of the desktop GPU. There are not enough calculations and memory transfers to utilize this GPU rationally. The proportionally high increase of the ARM-CPU on the Jetson board is due to lesser special arithmetic units on the CPU, which can calculate, the necessary trigonometric functions for the coordinate transformation, in hardware.

In Table 1, measurement results of the coordinate transformation with the minimum, maximum, average and median values are given. The discrepancy between the minimum and maximum value of one measurement is on the CPU much higher than on the GPU. The reason for that is, that on the CPU at the same time interrupts of the operating system, without user input, have to be handled. Instead, on the GPU, that is not the case. The much more steady executions times on the GPU are a further advantage, besides the speedup, because so the execution times are more predictable. The high discrepancy was observed at all of the experiments.

In the next experiment, we evaluate the execution times of the ego-motion compensation of the vehicle. As

Table 2: Average execution time of the coordinate transformation from polar to Cartesian space including bubble sort in *ms* on the Nvidia Jetson K1 board.

Number of laser channels	ARM-K1	K1-GPU	Speedup
581	0.51	0.25	2.0
1162	0.93	0.26	3.5
2324	1.59	0.32	5.0
5810	4.14	0.57	7.3

described in Section 2, the single sensor measurements can be directly compensated by the ego-motion of the vehicle. Again, for each laser beam, a CUDA thread was created. In Figure 6, the results of the experiments are shown.

The break-even point, where the GPU is faster than the CPU, is for the desktop computer by roundabout 60000 laser beams. For the Jetson K1 board, the break-even point is instead already by roundabout 10000 laser beams. The reason for the earlier break-even point on the Jetson board is that the performance ration between the desktop CPU and the desktop GPU is smaller than on the embedded board, due to the high performance of the desktop CPU. For a higher number of measurements the speedup, between the GPUs and the CPUs versions would further increase, in favor for the GPUs versions. At a certain point, the speedup curve would flatten out, if the GPU is fully utilized.

3.2.2 Novel Parallel Occupancy Grid Map

In Table 2, the results of the parallelization of the coordinate transformation, including the bubble sort, are shown. Only for every horizontal channel of the laser scanner a CUDA thread was created, due to the intrinsics of the bubble sort algorithm. The sorting of the vertical layers of one horizontal channel is done sequentially. A parallel sorting algorithm, like a bitonic sorter (Batcher, 1968), was not rational usable, due to the low number of vertical layers. The number of vertical layers would have to be increased to an unrealistic number (> 1000), that this algorithm would be efficient on a GPU. For every chosen resolution of the laser, a speedup on the GPU could be achieved. The speedups are only moderate because only for valid data a coordinate transformation was done and in real-world scenarios, which we used, quite a lot of data is not valid. The higher the number of laser beams, the higher the speedup is. The reason for this is that with a higher number of laser beams, in the sum more arithmetic operations and the GPU is better utilized.

Finally, the measurements have to be put into the occupancy grid map. For that experiment, we paralleli-

Table 3: Average execution time of the grid map update including the determination of static an d dynamic objects in *ms* on the Nvidia Jetson K1 board. For every channel (and not additionally for every layer) a CUDA thread is started.

Number of laser channels	ARM-K1	K1-GPU	Speedup
581	1.51	1.79	0.8
1162	2.41	1.81	1.4
2324	4.13	1.78	5.0
5810	12.3	1.82	7.2

Table 4: Average execution time of the grid map update including the determination of static an d dynamic objects in *ms* on the Nvidia Jetson K1 board. For every channel and for every layer a CUDA thread is started.

Number of laser channels/ Number of laser layers	K1-ARM	GPU-K1	Speedup
581/3	1.54	1.23	1.25
581/30	1.53	7.60	0.2
5810/3	11.96	4.92	2.43
5810/30	11.96	40.76	0.29

zed only the horizontal channels of the laser scanner. The resolution of the laser scanner in the vertical direction was always three. The results, therefore, are shown in Table 3. The speedup increases with the number of laser measurements, for the same reason mentioned above. The execution time on the CPU increases much more than on the GPU.

Since our laser scanner has not only laser beams in the horizontal layer, but also in the vertical layer, we created for every laser beam one thread. The result of this parallelization is shown in Table 4.

For 581 laser beams in the horizontal layer, the speedup was highe, than in the previous experiment, where only the horizontal layers were parallelized. If we increase the number of vertical layers, the GPU version is slower than the CPU version. The reason for that is our efficient algorithm. We have sorted the vertical layers of one horizontal layer in the order of the distance of the measurement. Only the measurement of the shortest distance to an object is evaluated. This means, a lot of threads are started on the GPU and then have nothing to do, which creates an overhead.

4 CONCLUSION

In this paper, we demonstrated for several base algorithms common in ADAS for automated driving, if and for which sensor resolutions they can be efficiently parallelized on a GPU. In almost all cases, the performance on the GPU increased with an increasing sensor resolution. The achieved speedups of the base algorithms were higher than the whole update algorithm, due to its less complex structure. Further, we presented, a novel approach for the parallelization of an occupancy grid map on a GPU. Therefore, we used the intrinsics characteristics of the thread execution model by the Nvidia framework CUDA and evaluated our approach with real-time data collected on a highway.

REFERENCES

Audi AG (2016). Everything combined, all in one place: The central driver assistance control unit. `http://www.audi.com/com/brand/en/vorsprung_durch_technik/content/2014/10/zentrales-fahrerassistenzsteuergeraet-zfas.html`.

Badino, H., Franke, U., Mester, R., and Main, F. A. (2007). Free space computation using stochastic occupancy grids and dynamic programming. In *In Dynamic Vision Workshop for ICCV*.

Bar-Shalom, Y., Daum, F., and Huang, J. (2009). The probabilistic data association filter. *IEEE Control Systems*, 29(6):82–100.

Batcher, K. E. (1968). Sorting networks and their applications. In *Proceedings of the Spring Joint Computer Conference (AFIPS)*, AFIPS '68 (Spring), pages 307–314, New York, NY, USA. ACM.

Bresenham, J. E. (1965). Algorithm for computer control of a digital plotter. *IBM Systems Journal*, 4(1):25–30.

Chen, C., Tay, C., Laugier, C., and Mekhnacha, K. (2006). Dynamic environment modeling with gridmap: A multiple-object tracking application. In *2006 9th International Conference on Control, Automation, Robotics and Vision*, pages 1–6.

Cover, T. and Hart, P. (2006). Nearest neighbor pattern classification. *IEEE Trans. Inf. Theor.*, 13(1):21–27.

Dryanovski, I., Morris, W., and Xiao, J. (2010). Multi-volume occupancy grids: An efficient probabilistic 3d mapping model for micro aerial vehicles. In *Proceedings of the IEEE/RSJ International Conference on Intelligent Robots and Systems (IROS)*, pages 1553–1559.

Elfes, A. (1989). Using occupancy grids for mobile robot perception and navigation. *Computer*, 22(6):46–57.

Fickenscher, J., Reiche, O., Schlumberger, J., Hannig, F., and Teich, J. (2016). Modeling, programming and performance analysis of automotive environment map representations on embedded GPUs. In *2016 IEEE International High Level Design Validation and Test Workshop (HLDVT)*, pages 70–77.

Grisettiyz, G., Stachniss, C., and Burgard, W. (2005). Improving grid-based slam with Rao-Blackwellized particle filters by adaptive proposals and selective resampling. In *Proceedings of the IEEE International Conference on Robotics and Automation*, pages 2432–2437.

Homm, F., Kaempchen, N., Ota, J., and Burschka, D. (2010). Efficient occupancy grid computation on the GPU with lidar and radar for road boundary detection. In *Proceedings of the IEEE Intelligent Vehicles Symposium*, pages 1006–1013.

Kalman, R. E. (1960). A new approach to linear filtering and prediction problems. *Transactions of the ASME–Journal of Basic Engineering*, 82(Series D):35–45.

Kammel, S. and Pitzer, B. (2008). Lidar-based lane marker detection and mapping. In *Proceedings of the IEEE Intelligent Vehicles Symposium*, pages 1137–1142.

Moravec, H. (1988). Sensor fusion in certainty grids for mobile robots. *AI Mag.*, 9(2):61–74.

Moravec, H. (1996). Robot spatial perception by stereoscopic vision and 3d evidence grids. Technical Report CMU-RI-TR-96-34, Carnegie Mellon University, Pittsburgh, PA, USA.

Musicki, D. and Evans, R. (2004). Joint integrated probabilistic data association: Jipda. *IEEE Transactions on Aerospace and Electronic Systems*, 40(3):1093–1099.

NVIDIA Corp. (2016a). NVIDIA Jetson TK1 Developer Kit. `http://www.nvidia.com/object/jetson-tk1-embedded-dev-kit.html`.

NVIDIA Corp. (2016b). Programming guide – CUDA toolkit documentation. `https://docs.nvidia.com/cuda/cuda-c-programming-guide/`.

Sebastian Thrun, Wolfram Burgard, D. F. (2005). *Probalistic Robotics*. The MIT Press, Cambridge, Massachusetts and London, England.

Werber, K., Rapp, M., Klappstein, J., Hahn, M., Dickmann, J., Dietmayer, K., and Waldschmidt, C. (2015). Automotive radar gridmap representations. In *2015 IEEE MTT-S International Conference on Microwaves for Intelligent Mobility (ICMIM)*, pages 1–4.

Yguel, M., Aycard, O., and Laugier, C. (2006). Efficient gpu-based construction of occupancy girds using several laser range-finders. In *Intelligent Robots and Systems, 2006 IEEE/RSJ International Conference on*, pages 105–110.